The variable 6307Å emission line in the spectrum of Eta Carinae: blueshifted [S III] λ6313 from the interacting winds

T. R. Gull[1]

ABSTRACT

The 6307Å emission line in the spectrum of η Car (Martin et al. 2006) is blueshifted [S III] λ6313 emission originating from the outer wind structures of the massive binary system. We realized the identification while analyzing multiple forbidden emission lines not normally seen in the spectra of massive stars. The high spatial and moderate spectral resolutions of *HST*/STIS resolve forbidden lines of Fe^{+}, N^{+}, Fe^{+2}, S^{+2}, Ne^{+2} and Ar^{+2} into spatially and velocity-resolved rope-like features originating from collisionally-excited ions photo-ionized by UV photons or collisions. While the [Fe II] emission extends across a velocity range of $\pm$500 km s^{-1} out to 0.″7, more highly ionized forbidden emissions ([N II], [Fe III], [S III], [Ar III], and [Ne III]) range in velocity from $-$500 to +200 km s^{-1}, but spatially extend outward to only 0.″4. The [Fe II] defines the outer regions of the massive primary wind. The [N II], [Fe III] emission define the the outer wind interaction regions directly photo-ionized by far-UV radiation. Variations in emission of [S III] $\lambda\lambda$9533, 9071 and 6313 suggest density ranges of 10^6 - 10^{10} cm^{-3} for electron temperatures ranging from 8,000 to 13,000° K. Mapping the temporal changes of the emission structure at critical phases of the 5.54-year period will provide important diagnostics of the interacting winds.

Subject headings: stars: binaries:spectroscopic, stars: individual: Eta Carinae, stars:winds

1. Introduction

Martin et al. (2006) found a variable emission line centered at 6307Å in multiple spectra of η Car, recorded by *HST*/STIS and by *VLT*/UVES. They were unable to identify the origin of the emission line, but demonstrated that the line was present across the high state

[1]Laboratory for Extrasolar Planets and Stellar Astrophysics, Exploration of the Universe Division, Code 667, Goddard Space Flight Center, Greenbelt, MD 20771

(defined by presence of forbidden lines of doubly-ionized elements, see Damineli et al. (2008) and references therein) and disappeared during the low state.

Recently Gull et al. (2009), using the same spectra, focused on the spatially-extended forbidden line emission both from high-ionization (herein defined as >14 eV) and low-ionization (8-13 eV). We found that the forbidden emission originated from 1) the Weigelt condensations (Weigelt & Ebersberger 1986), as narrow lines centered on -43 km s^{-1}, 2) the boundaries of the primary wind (η Car A) as rope-like [Fe II], photo-ionized by mid-UV and collisionally excited at densities around N_e=10^7cm^{-3}, and 3) the wind interaction region, as high-ionization emission from [N II], [Fe III], [Ar III], [Ne III] and [S III], photo-ionized by far-UV and collisionally excited for densities, n_e ranging from 10^5 to 10^8cm^{-3}. The high-ionization emission lines are present both for the Weigelt condensations and the wind interaction region during the 5 year high state, but every 5.5 years, disappear during the low state. X-ray models (Pittard & Corcoran 2002; Parkin et al. 2009) place the binary periastron event near the onset of the low state with a three to six month recovery.

We applied a 3D SPH (smoothed particle hydrodynamics) model (Okazaki et al. 2008) extended out to 1700 AU (0.″67) to match the spatial structure seen in these forbidden lines and realized that the bulk of the high-ionization emission structure originated from the wind interaction region in the outer portion of the massive wind structure. We found that portions of the wind interaction structure, moving ballistically outward, are directly illuminated by the far-UV radiation of the hot secondary, η Car B, leading to highly-ionized, collisionally excited gas and hence the high-ionization extended emission.

Further examination of the *HST*/STIS longslit spectra showed that the previously unidentified emission at 6307Å is blue-shifted [S III] λ6313 emission from the interacting wind structure. The evidence is subtle, but convincing. We summarize the observations in Section 2. A description of how the spectro-images were produced is in Section 3. The forbidden emission structures are described in Section 4. Discussion in Section 5 provides insight on the ionization and excitation leading to [S III] emission and the potential for monitoring changes with orbital phase, including mapping temperature with density dependence. We conclude with a summary in Section 6. Throughout this paper, all wavelengths are in vacuum, the velocities are heliocentric, directions are compass points (N=north, NNW= north by northwest and the phase of the binary orbit is referenced to the X-ray minimum beginning at 1997.9604 (Corcoran 2005).

2. The *HST*/STIS Observations

The spectra discussed here are a portion of the Eta Carinae Treasury observations accessible through the STScI archives (http://archive.stsci.edu/prepds/etacar) as reduced by a special reduction tool developed by K. Ishibashi and K. Davidson. For brevity we focus on two sets of observations, recorded in July 2002 (ϕ=0.820) and July 2003 (ϕ=1.001).

Observations were recorded with the *HST*/STIS moderate dispersion gratings and CCD detector through the $52''\times0''.1$ aperture. We wanted to monitor the change in both η Car and the Weigelt condensations (Weigelt & Ebersberger 1986), which drop in excitation during the low state. However the range in aperture position angle (PA) is limited by the required orientation of *HST* solar panels and changes throughout the year. can prevent inclusion of any one of the three Weigelt condensations within the aperture when centered on η Car (Figure 1). For observations centered around the X-ray minimum, predicted to be around 1 July, 2003, we scheduled a visit one year earlier, July 2, 2002 (orbital phase, ϕ=0.820), at a pre-selected PA=69°, that would be accessible just before(ϕ=0.995) and after the X-ray minimum (ϕ=1.001). During all three visits, separate observations centered on η Car and Weigelt D were obtained with the aperture placed as shown in Figure 1. Additional information on the observations are presented in Martin et al. (2006) and Gull et al. (2009).

3. Spatially-resolved Emission

The *HST*/STIS spatial-resolution ($0''.1$ at Hα) separates the spectrum of η Car's core from extended structures, especially the narrow line emission that originates from the Weigelt condensations (Davidson et al. 1995), located between $0''.1$ to $0''.3$ in the NW quadrant relative to η Car (see Figure 1). As described by Gull et al. (2009), we found considerable differences between many broad forbidden emission line profiles of η Car as recorded by the *VLT*/UVES and the *HST*/STIS. Extractions with a $0''.127$-high slice of the STIS spectra (five half rows in the reduced spectro-images) yielded broad wind line profiles for H I, He I and Fe II lines that compared favorably with those recorded by *VLT*/UVES. In contrast, broad profiles of forbidden lines recorded by *VLT*/UVES were nearly absent in the *HST*/STIS extractions centered on η Car. Examination of the *HST*/STIS long aperture spectra revealed faint structure in these emission lines extending out to $0''.7$. However, the observed emission was highly variable both with aperture PA and orbital phase, ϕ. Clearly the forbidden line emission is spatially extended on scales resolved by *HST*/STIS but not by *VLT*/UVES.

We examined individual lines in more detail and attempted to enhance visibility of the extended line emission by several reduction procedures. While various spatial filters were tried, the best results were obtained by subtraction of measured continuum on a spatial

row-by-row basis. We used spectral plots of the Weigelt condensations (Zethson 2001) to identify 10 to 20Å intervals with no obvious presence of narrow or broad line emission. At each position along the aperture, we measured and subtracted the average continuum in that spectral interval. Examples of the resulting spectro-images (intensity images with x=velocity and y=angular size) are presented in Figure 2.

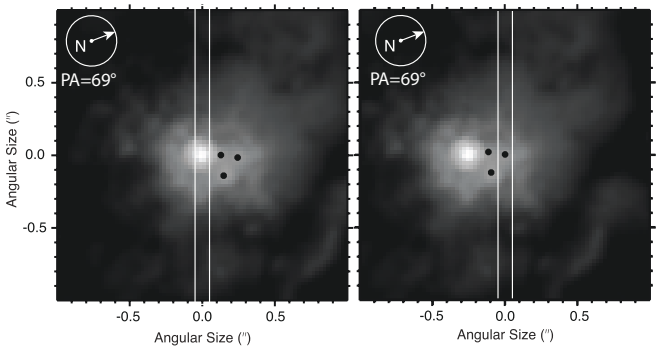

Fig. 1.— *HST*/**STIS aperture positions: Left:** Centered on η Car. **Right:** Centered on Weigelt D. The $2''\times2''$ Field of View is extracted from an *HST*/ACS image recorded in February 2003 through the 550M filter. Weigelt condensations B, C and D are indicated by the black dots. The projection of the $52''\times0\farcs1$ aperture is indicated. Note the field is rotated by 69° placing the aperture vertical. North is indicated by the compass.

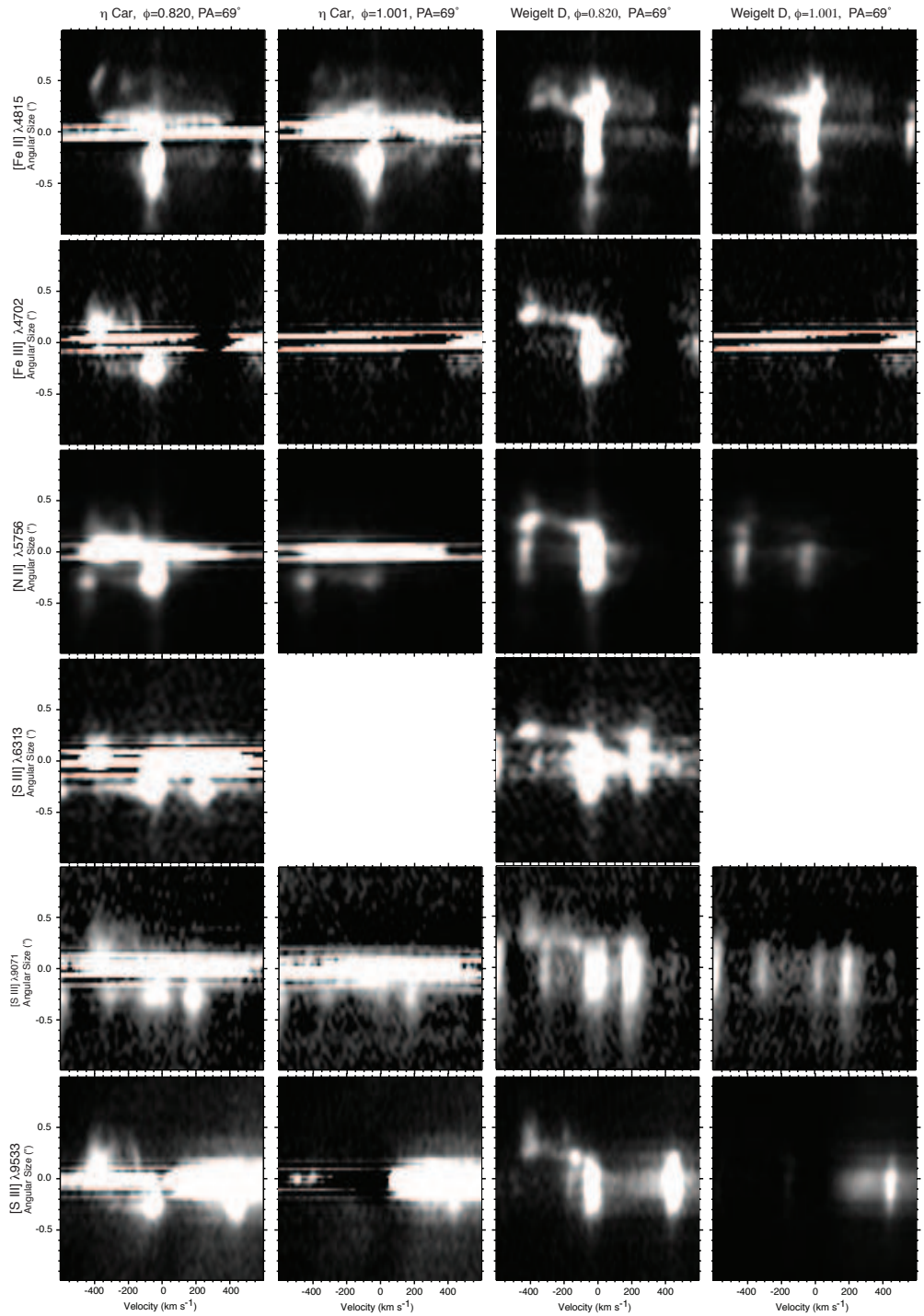

Fig. 2.— **Spectro-images** centered on η Car (Columns 1 and 2) and on Weigelt D (Columns 3 and 4). **[Fe II] λ4815** (Row 1) **[Fe III] λ4703** (Row 2) **[N II] λ5756** (Row 3) and **[S III] λλ6313, 9071, 9533** (Rows 4–6) **Note:** Continuum in regions free of narrow or broad-line emission has been subtracted on a spatial line-by-line basis to display the extended emission structure. All plots are with a grey level proportional to $\sqrt{Intensity}$. All observations were recorded with PA=69°.

These spectro-images provide only a qualitative view of the line profile. We caution the reader that quantitative measures require much more precision for the following reasons:

1. The STIS utilized a three-axis mechanism to select a grating and to set the correct tilt angle for the spectral interval of choice. While return to that grating position is within a few CCD pixels, variations in the tilt are not fully reproducible. A tilt of 1/20 pixel along the 1024 element row led to significant photometric variation when attempting to extract spectra at the 0.″1 spatial resolution.

2. The standard calibration for the STIS photometry is properly referenced to extractions of a stellar spectrum with a 2″-wide aperture, allowing for full capture of flux from a point source. Apertures with widths comparable to the diffraction limit of *HST* sample the point spread function of the telescope, which changes dynamically even within an orbit.

3. Charge transfer inefficiency (CTI) leads to a trail in the direction of columns and, with on-orbit time, increases. For complex sources like extended structures, a proper extraction is not available.

These problems complicate attempts to show extended structure in the vicinity of a bright star, which is exactly the situation with η Car. This leads to the obvious linear striations at the star position in the spectrally-dispersed (velocity) coordinate. These variations do affect measures of the extended emission closest to the stellar position. However, for offsets to Weigelt D, the stellar flux is blocked by the aperture, and quantitative measures are then possible. We note that the stellar spectrum scattered from the direction of Weigelt D is very different from the direct spectrum of η Car. The lack of P Cygni absorption in Hα across the high state indicates fully-ionized hydrogen in the region spatially located between η Car and Weigelt D (Gull et al. 2009). On the side of caution, we limit this discussion to a description of the spatial and velocity structure of the lines. Even with qualitative descriptions, we gain much insight on the spatially resolved wind interactions and the source of the 6307Å emission.

4. Description of the emission structures

We refer the reader to Figure 2 for the following descriptions of the forbidden line emission. The first two columns of spectro-images are extracted from spectra centered on η Car in the high state (ϕ=0.820) and early in the low state (ϕ=1.001). Likewise, columns 3 and 4 are centered on Weigelt D (A more complete summary on variation of the emission

structures with ionization potential and orbital phase is presented by Gull et al. (2009)).

Four basic structures contribute to these spectro-images:

1. The central core of η Car, not resolved by *HST* at 0.″1, which contributes the bulk of the continuum and P Cygni wind lines, notably of H I and Fe II.

2. Weigelt D and other, lesser condensations that contribute many narrow emission lines centered at -40 km s^{-1}.

3. Rope-like structures of high-ionization forbidden emission lines with velocity components extending from +200 to -500 km s^{-1}.

4. Noticeably more-diffuse, rope-like structures of low-ionization forbidden emission lines, specifically [Fe II].

Spectro-images of [Fe II] λ4815 (Row 1) show narrow rope-like features extending to 0.″7 at -500 km s^{-1}and other, more diffuse structures closer to the star extending $\pm$500 km s^{-1}. The narrow emission at -40 km s^{-1} originates from extended structure WSW of η Car, not noted by Weigelt & Ebersberger (1986), but present throughout the observational period from 1999 to 2004 whenever the STIS aperture sampled this position. The narrow [Fe II] emission centered on Weigelt D extends 0.″5 E and W of Weigelt D, but at about 0.″25 E of D, a diffuse emission extends to -400 km s^{-1}and away from η Car. During the low state, the outer [Fe II] emission drops, becomes more diffuse and is located closer to η Car.

The [Fe III] λ4703 (Row 2) is interior to the rope-like [Fe II] λ4815. A series of highly filamentary loops extend from η Car to the east at velocities from -40 to -500 km s^{-1}. No red-shifted velocity components are seen at this PA. However, Gull et al. (2009) find that at PA=-28°, observed six times from 1998.0 to 2004.3 (ϕ=0.000 to 1.122), red-shifted components extend to +200 km s^{-1} at early phases, but fade late in the high state. All [Fe III] λ4703 disappears during the low state.

The [N II] λ5756 (Row 3) has very similar structure to that of [Fe III] λ4703 with higher S/N. A narrow emission line, [Fe II] λ5748, appears at the -550 km s^{-1} position and persists in the low state, along with weak [N II] λ5756. The structure of [N II] λ5756 extends from -40 to -500 km s^{-1} in the spectro-image centered on Weigelt D during the high state, but also disappears in the low state.

Three [S III] lines are shown in Rows 4–6 as each is important in accounting for the 6307Å emission. Unfortunately, the [S III] λ6313 (Row 4) was recorded only at ϕ=0.820, but the other two lines were observed at both phases. Most noticeable in the spectro-image of η Car at ϕ=0.820 is a knot of emission, centered on the stellar position at -400 km s^{-1}. The effective wavelength is 6307Å. That spectral interval was recorded at other phases, but at

other position angles, during the 2003.5 minimum with no [S III] λ6313 present either at the positions of η Car or Weigelt D. The extended structure is less apparent in the spectro-image of η Car at ϕ=0.820, but is well-defined in the spectro-image centered on Weigelt D. Narrow lines of [O I] λ6302, Fe II $\lambda\lambda$6307, 6309 and 6319 contaminate the spectro-image and persist during the minimum.

The [S III] λ 9071 (Row 5) weak emission extends off of η Car, but several narrow lines (N I λ9063, Fe II λ9073) also contribute to the spectro-image. The high-velocity arc of [S III] λ 9071 extends blueward from Weigelt D.

The [S III] λ9533 emission (Row 6) is quite similar to that of [Fe II] λ4703 (Row 2) and confirms that [S III] emission extends to -500 km s^{-1}. The bright emission to the red of [S III] λ9533 is H I Pa 8 λ9548, which originates primarily from the central core.

5. Discussion

We associate the low-ionization structure with the massive, slow-moving wind of η Car A. The high-ionization emission is from the interacting wind region piled up by the fast-moving, less-massive wind of η Car B (Pittard & Corcoran 2002). The bulk of the interacting wind, by its velocity, appears to be mostly ionized wind of η Car A. The higher velocity side of the shock is likely less dense and more highly ionized by η Car B.

Using the 3D SPH models of Okazaki et al. (2008) and simple geometric models, we determined that the high-ionization emission originates from a distorted paraboloidal structure lying in the skirt of the Homunculus. Based upon the blue-shifted velocities and near symmetry for PAs ranging from +22 to +38°, the paraboloid points in our general direction with axis of rotation projecting onto the sky at PA$\approx -25°$.

Martin et al. (2006) performed a very complete analysis on the unidentified 6307Å line in both the *HST*/STIS and *VLT*/UVES spectra, finding very similar behavior with orbital phase. Their search of possible line identifications focused primarily on singly-ionized species such as Fe^+, V^+ and S^+, although they do list [S III] as a narrow nebular line identified by Zethson (2001) in the spectrum of the Weigelt condensations. Their candidate of greatest interest appeared to be Fe III] λ6306.43 with unknown atomic data for the transition.

Most important in their analysis was the tracking of the strength of the emission throughout the 5.5-year orbit. They found that the line disappeared during the low state, but might be anti-correlated with Fe II λ5529. Both suggest a high-ionization source. Nielsen et al. (2007) analyzed the behavior of the He I absorption, finding an anti-correlation with Fe II absorption.

Salient are three facts:

1. On the star, both *HST*/STIS and *VLT*/UVES see the same emission bump with similar strengths.

2. The emission correlates with high-ionization variations, not the behavior of the low-ionization emission of Fe II.

3. The extended emission of the extended emission correlated with [S III] correlates very well with the extended emission identified with [S III] $\lambda\lambda$9071 and 9533.

6. Conclusions

We have presented conclusive evidence that the emission line at 6307Å, noted in the spectra of η Car by Martin et al. (2006) is blue-shifted emission of [S III] λ6313 originating from the distorted paraboloidal, interaction region located between the massive binary members. While the massive primary, η Car A, provides the dominant wind ejecta, 10^{-3} $M_{\odot}$/y at 500 km s^{-1}, the hotter secondary provides a less massive, faster wind, 10^{-5} $M_{\odot}$/y at 3000 km s^{-1}, and far-UV photons that ionize iron, neon, argon and sulfur to doubly ionized states. Thermal collisions, mid-UV photons and possible charge exchange excite the doubly-ionized species to upper states with forbidden transitions leading to forbidden line emission in regions with densities close to n_c. Specifically, [S III] $\lambda\lambda$9533, 9071 and 6313 have extended spatial structures. The intensity ratio (Flux (λ9533) + Flux (λ9071)/Flux(λ6313) leads to density estimates ranging from 10^7 - 10^8 cm^{-3}on the scale of 0.″1, the limit of *HST*/STIS spatial capabilities. Mapping in these and other doubly-ionized lines will provide powerful measures for models of wind interactions using various 3-D hydrodynamical codes.

The observations were accomplished with the NASA/ESA Hubble Space Telescope. Support for Program numbers 7302, 8036, 8483, 8619, 9083, 9337, 9420, 9973, 10957 and 11273 was provided by NASA directly to the Space Telescope Imaging Spectrograph Science Team and through grants from the Space Telescope Science Institute, which is operated by the Association of Universities for Research in Astronomy, Incorporated, under NASA contract NAS5-26555. All analysis was done using STIS IDT software tools on data available through the *HST* η Car Treasury public archive.

REFERENCES

Corcoran, M. F. 2005, AJ, 129, 2018

Damineli, A., Hillier, D. J., Corcoran, M. F., & et al. 2008, MNRAS, 384, 1649

Davidson, K., Ebbets, D., Weigelt, G., Humphreys, R. M., Hajian, A. R., Walborn, N. R., & Rosa, M. 1995, AJ, 109, 1784

Gull, T. R., Nielsen, K. E., Corcoran, M. F., Madura, T. I., Owocki, S. P., Russell, C. M. P., Hillier, D. J., Hamaguchi, K., Kober, G. V., Weis, K., Stahl, O., & Okazaki, A. T. 2009, MNRAS, accepted

Martin, J. C., Davidson, K., Humphreys, R. M., & et al. 2006, ApJ, 640, 474

Nielsen, K. E., Corcoran, M. F., Gull, T. R., & et al. 2007, ApJ, 660, 669

Okazaki, A. T., Owocki, S. P., Russell, C. M. P., & Corcoran, M. F. 2008, MNRAS, 388, L39

Parkin, E. R., Pittard, J. M., Corcoran, M. F., Hamaguchi, K., & Stevens, I. R. 2009, MNRAS, in press

Pittard, J. M. & Corcoran, M. F. 2002, A&A, 383, 636

Weigelt, G. & Ebersberger, J. 1986, A&A, 163, L5

Zethson, T. 2001, PhD thesis, Lund University